Supporting Information for:

Guanidinium-Formamidinium Lead Iodide: A Layered Perovskite-Related Compound with Red Luminescence at Room Temperature

Olga Nazarenko[†,‡], Martin R. Kotyrba[†,‡], Sergii Yakunin[†,‡], Marcel Aebli[†,‡], Gabriele Rainò,[†,‡] Bogdan M. Benin, [†,‡] Michael Wörle[†], Maksym V. Kovalenko[†,‡]*

† Laboratory of Inorganic Chemistry, Department of Chemistry and Applied Bioscience, ETH Zürich, Vladimir Prelog Weg 1, CH-8093 Zürich, Switzerland

‡ Laboratory for Thin Films and Photovoltaics, Empa – Swiss Federal Laboratories for Materials Science and Technology, Überlandstrasse 129, CH-8600 Dübendorf, Switzerland

[*]E-mail: mvkovalenko@ethz.ch

1. Materials and Methods

Chemicals. Lead (II) acetate ($Pb(OAc)_2 \times 3H_2O$, ≥99.99%) was purchased from Sigma Aldrich. Guanidinium carbonate (G_2CO_3, 99+%) was purchased from Acros. Hydrogen iodide (HI, 57%, stabilized with 1.5% hypophosphorous acid, H_3PO_2) and formamidinium acetate (FA(OAc), 99%) were received from ABCR. Diethyl ether was used from different sources. Toluene (> 99.7%) was purchased from Fisher. All chemicals were used as received without further purification.

Method 1. $FAGPbI_4$ was crystallized from hot hydroiodic acid solution. FA(OAc) (4 mmol), G_2CO_3 (4 mmol) and $Pb(OAc)_2 \times 3H_2O$ (4 mmol) were loaded into a 25-ml round-bottom flask equipped with a magnetic stirring bar and a septum. The flask was then cooled with an ice bath, followed by the addition of HI (18 mL). Gas evolution was observed, while a mixture of brown and yellow precipitates formed. This mixture was heated with a glycerol bath (50-55 °C) with magnetic stirring until a clear yellow solution formed. Then the solution was cooled to room temperature (RT), the stirring was stopped and the stirring bar removed. After a few hours, small brown crystals appeared. Crystals were allowed to crystallize for an additional 12 h and then were separated by vacuum filtration and washed with diethyl ether and toluene. Finally, the product was dried in a vacuum oven (10-50 mbar) overnight at 55 °C. A yield of 14 % was estimated relative to the initially loaded $Pb(OAc)_2 \times 3H_2O$. To grow larger crystals (few mm), the initially obtained smaller crystals were carefully introduced into another vessel with a fresh reaction mixture (at the point of cooling it to RT), and left undisturbed for 1-2 days, followed by washing with diethylether and toluene.

Method 2 (higher yield). FA(OAc) (6.75 mmol) G_2CO_3, (4.5 mmol) and $Pb(OAc)_2 \times 3H_2O$ (4.5 mmol) were loaded into a 50-ml round-bottom flask equipped with a magnetic stirring bar and a septum. The mixture was cooled with an ice bath, and 20 ml of HI was added. A mixture of yellow and brown precipitates formed immediately, which fully dissolved upon further heating with a glycerol bath (60-70 °C) forming a clear yellow solution. During cooling to RT a yellow precipitate crystallized out. At RT, yellow needles began to redissolve and dark brown needles appeared. After *ca.* 1-2 h, the mixture was shaken to promote complete dissolution of the yellow precipitate (that remains below brown crystals). After 5 hours, the brown product was separated by vacuum filtration and washed with diethylether and toluene. A yield of 40 % was estimated relative to the initially loaded $Pb(OAc)_2 \times 3H_2O$.

Reference compounds for characterization of FAGPbI$_4$ by ^{207}Pb ssNMR.

G$_2$PbI$_4$ was obtained as yellow platelets from a hot acidic solution using $[C(NH_2)_3]_2CO_3$ (3 mmol), PbI_2 (2 mmol) and 7.5 ml of HI (57%). The crystals were separated by vacuum filtration, washed with diethyl ether and dried in a vacuum oven at 60 °C. A yield of 30 % was estimated relative to the initially loaded PbI_2.

α-FAPbI$_3$. The synthetic procedure was adapted from Saidaminov *et al.*[1] The concentration of [Pb] and [FA] were adjusted to 1 M. Black crystals of α-FAPbI$_3$ were taken out from the hot gamma-butyrolactone solution, dried with a filter paper and annealed under inert condition (Ar atmosphere) at 180 °C for 2 h. Crystals were then kept at 120 °C (overnight) until the ^{207}Pb NMR measurement was conducted.

δ-FAPbI$_3$ was crystallized from hot HI acid. For this FA(OAc) (1 mmol) and $Pb(OAc)_2 \times 3H_2O$ (1 mmol) were dissolved in 3 ml of hot HI acid. A clear yellow solution resulted, and the solution was cooled to RT. A yellow product crystallized out upon cooling to RT. This was isolated by vacuum filtration, rinsed with diethyl ether and dried in a vacuum oven at 50 °C. A yield of 30 % was estimated relative to the initially loaded $Pb(OAc)_2 \times 3H_2O$.

2. Characterization

Powder X-ray diffraction (XRD) patterns were collected in transmission mode with a STADI P diffractometer (STOE&Cie GmbH), equipped with a curved Ge (111)-Monochromator (CuK$_{\alpha 1}$=1.54056Å) and a silicon strip MYTHEN 1K Detector (Fa. DECTRIS). For the measurement, ground powder was placed between adhesive tape.

Single-crystal XRD measurements were conducted on Bruker Smart Platform diffractometer equipped with a Apex I CCD detector and molybdenum (MoKα=0.71073 Å) sealed tube as an X-ray source. Crystals were tip–mounted on a micromount with paraffin oil. The data was processed with APEX3 (Bruker software)[2], structure solution and refinement was performed with SHELXS[3] and SHELXL[4] respectively, embedded in the Olex2 package.[5] For twin indexing the cell_now algorithm (a part of the Bruker APEX3 software package) was used.

The crystal structure of the synthesized compound was solved with direct methods, light elements (C, N) were located in the difference Fourier map, most of the positions of the cations were refined as rigid groups, and hydrogen atoms were placed at calculated positions.

UV-Vis absorbance spectra of the microcrystalline powders were collected using a Jasco V670 spectrophotometer equipped with deuterium (D$_2$) lamp (190 – 350 nm) for use in UV, a halogen lamp (330 – 2700 nm) for use in UV/NIR, and an integrating sphere (ILN-725) with a working wavelength range of 220 – 2200 nm. The absorbance spectra were estimated from diffuse reflectance measured on the powdered crystals transformed into Kubelka-Munk function.

Photoluminescence spectra were measured in a Joule–Thomson cryostat (MMR Technologies) operated in the temperature range of 78-300 K. PL emission was recorded with a heating rate of approximately 5 K/min. A 405 nm diode laser with the wavelength of 405 nm was used for excitation. Scattered laser emission was filtered out using dielectric long-pass filters with edges at 400 and 450 nm, respectively. The emission from the samples was collimated to an optical fiber and recorded at 1 K intervals with a CCD spectrometer LR1 (Aseq Instruments). PL spectra were corrected to the spectral sensitivity of the setup using Planck irradiation from a calibrated halogen lamp. Time-resolved photoluminescence (TR-PL) measurements were performed using a time-correlated single photon counting (TCSPC) setup, equipped with a SPC-130-EM counting module (Becker & Hickl GmbH) and an IDQ-ID-100-20-ULN avalanche photodiode (Quantique) for recording the decay traces. The emission was excited by a BDL-488-SMN laser (Becker & Hickl) with a pulse duration of 50 ps and wavelength of 486 nm, the CW power equivalent of ~0.5 mW, externally triggered at a 1 MHz repetition rate. PL emission from the samples passed through a long-pass optical filter with an edge at 500 nm in order to reject the excitation laser line. Average radiative lifetimes were determined as: $\tau_{avg} = \frac{\sum_{i=1}^{2} \tau_i^2 \cdot A_i}{\sum_{i=1}^{2} \tau_i \cdot A_i}$, where A_i and τ_i are corresponding amplitudes and exponential decay parameters in biexponential analysis. Absolute values of photoluminescence quantum yield (PLQY) was measured at Quantaurus-QY spectrometer from Hamamatsu in powder mode.

Micro-photoluminescence spectra were recorded in a home-built setup. The sample, i.e. a single crystal of FAGPbI$_4$, was mounted on xyz positioning stages (SmarAct, SLS 32:32; 1 nm resolution). A 405 nm laser diode (PicoQuant, LDH- D-C-405; repetition rate=2.5 MHz; excitation power density=90μJcm^{-2}) was focused on the sample by an oil immersion objective (Olympus, 100X; NA=1.4). PL was recorded by the same objective and analyzed by a monochromator (500 mm focal length; 300 lines/mm grating) coupled to an EMCCD camera (Princeton Instruments ProEM: 1600x400B_eXcelon3). For time-resolved PL, a single photon avalanche diode (PicoQuant PDM, 50 ps time resolution) was coupled at the exit port of the monochromator. TRPL traces were recorded by using a time-correlated single photon counting (TCSPC) module (PicoQuant, PicoHarp 300).

Photoconductivity measurements were performed with illumination from a tungsten lamp dispersed by an Acton SP2150 (Roper Scientific) spectrograph/monochromator. The light was modulated by a mechanical chopper at a frequency of 9 Hz. The sample was contacted by soft conductive rubber from opposite sides along the shorter axis of the crystal and biased at 100 V through these contacts using a Keithley 236 SMU. The signal, amplitude, and phase were measured across a series resistance by a Stanford Research 830 lock-in amplifier. The light intensity was controlled by a calibrated power detector (UM9B-BL, Gentec-EO).

Thermal analysis (thermogravimetry (TG) and differential scanning calorimetry (DSC)) was performed using a Netzsch Simultaneous Thermal Analyzer (STA 449 F5 Jupiter). A powdered sample (15.8 mg) was placed in an alumina crucible and heated under Ar gas flow (50 ml/min) to 800 °C (10 °C min^{-1}).

^{207}Pb solid-state NMR. All experiments were performed on a Bruker spectrometer (16.4 T) equipped with a 2.5 mm triple-channel solid-state probe head and an Avance III console. A 2.5 mm zirconia rotor was used. The spinning frequency was set to 20 kHz except for α-FAPbI$_3$ which was measured in static mode. Chemical shifts were referenced to PbMe$_4$. A Hahnecho pulse sequence was used. The 90-degree pulse had a length of 5 μs. The echo delay was set to 1 rotor cycle and the recycle delay to 0.5-2 seconds. For every spectrum, between 5'000 and 786'432 scans were recorded.
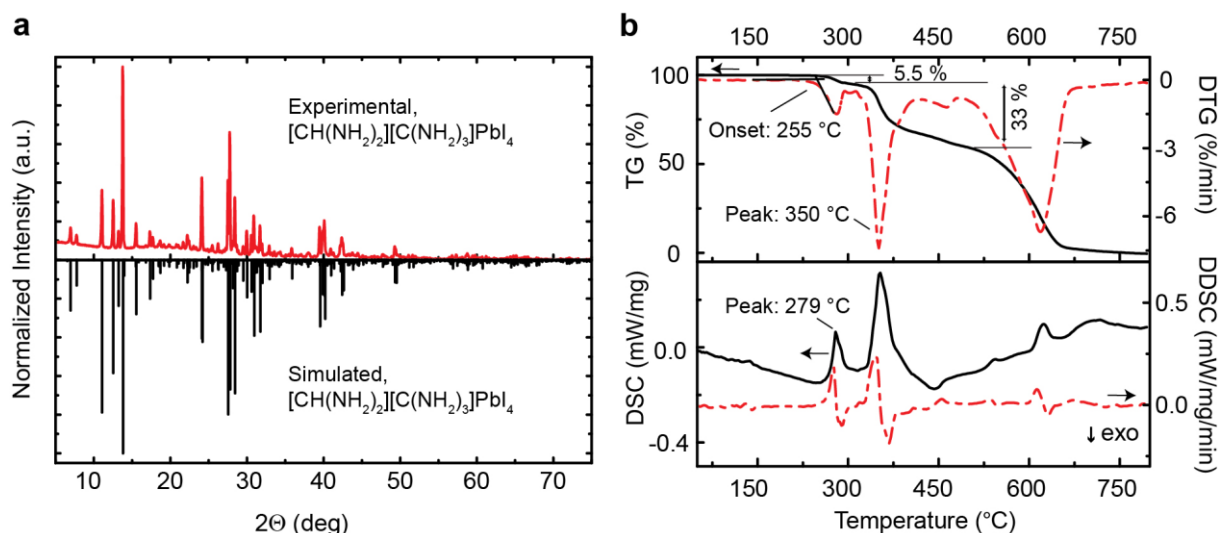
Figure S1. (a) Powder XRD pattern of FAGPbI$_4$ compared to the calculated pattern based on single crystal X-ray diffraction measurements. A preferred orientation of the microcrystalline powder is observed through the difference in intensity of certain reflections in the experimental pattern comparing to the calculated data due to the fact that FAGPbI$_4$ crystallizes in the shape of thin needles, giving rise to preferred orientation on a flat sample holder. (b) Thermal analysis of FAGPbI$_4$: thermogravimetric analysis (TG), differential scanning calorimetry (DSC) and corresponding derivatives (DTG, DDSC).

The first step of decomposition of FAGPbI$_4$ in the temperature range of 255 - 300 ℃ with a mass loss of about 5.5 % could correspond to the loss of formamidine. A weight percent (w) of formamidine (CN$_2$H$_4$) in FAGPbI$_4$ is 5.4 %. Next steps of decomposition are not clearly defined, as a further loss of organic part [guanidine, products of its fragmentation, w(guanidine, CN$_3$H$_5$) = 7.2 %] and HI, as well as sublimation of lead iodide take place.

Table S1. Crystallographic data for FAGPbI$_4$.

	[C(NH$_2$)$_3$][CH(NH$_2$)$_2$]PbI$_4$
Formula weight	819.95
Temperature (K)	298
Crystal system	monoclinic
Space group	*C*2/*m*
Color	brown
a (Å)	26.948(2)
b (Å)	12.8189(11)
c (Å)	14.4080(12)
α (°)	90
β (°)	109.9408(14)
γ (°)	90
Volume (Å^3)	4678.7(7)
Z	12
ρ$_{calc}$ (g/cm^3)	3.492
μ (mm^{-1})	18.710
F(000)	4224.0
Crystal size (mm^3)	0.32×0.06×0.04
Radiation	MoKα (λ = 0.71073)
2Θ range for data collection (°)	3.006 to 52.738
Index ranges	-33≤h≤33, -16≤k≤16,

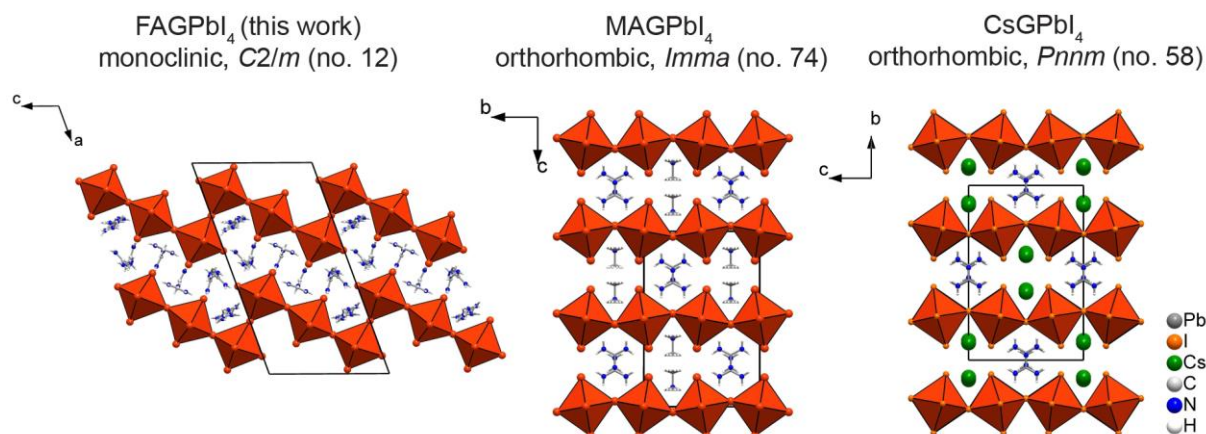|	−18≤l≤18
Reflections collected	21674
Independent reflections	5009 [R_{int} = 0.0386, R_{sigma} = 0.0319]
Data/restraints/para-meters	5009/0/144
Goodness-of-fit on F^2	1.074
Final R indexes [I>=2σ (I)]	R_1 = 0.0409, wR_2 = 0.0945
Final R indexes [all data]	R1 = 0.0552, wR_2 = 0.1016
Largest diff. peak/hole (e Å^{-3})	1.87/-1.27

Figure S2. Crystal structures of $FAGPbI_4$, $MAGPbI_4$ (Ref. 15 of the Main Text) and $CsGPbI_4$.

$MAGPbI_4$ as well as $CsGPbI_4$ belong to Ruddlesden-Popper-related phases. Ruddlesden-Popper phases are composed of (100) perovskite slabs with a general formula of $A_{n+1}B_nX_{3n+1}$ and a simplest member (n=1) adopting the K_2NiF_4 structure. The slabs in Ruddlesden-Popper phases are displaced by a vector (**a**+**b**)/2 with respect to each other. In the case of $MAGPbI_4$ as well as $CsGPbI_4$ the displacement is **a**/2.

Table S2. Fractional atomic coordinates and isotropic or equivalent isotropic displacement parameters (Å^2). The labeling of the atoms is illustrated in the screen shot below.

	x	y	Z	U_{iso}*/U_{eq}	Occ. (<1)
Pb1	0.2500	0.2500	0.5000	0.03861 (13)	
Pb2	0.36972 (2)	0.24941 (3)	0.17333 (3)	0.03893 (11)	
I1	0.14363 (3)	0.27884 (7)	0.31678 (6)	0.0661 (2)	
I2	0.22996 (5)	0.0000	0.48564 (10)	0.0679 (3)	
I3	0.31523 (3)	0.23463 (7)	0.35085 (6)	0.0633 (2)	
I4	0.36981 (5)	0.0000	0.13945 (9)	0.0706 (3)	
I5	0.47971 (3)	0.21806 (6)	0.33598 (6)	0.0572 (2)	
I6	0.41596 (3)	0.27989 (7)	0.00697 (6)	0.0656 (2)	
I7	0.2500	0.2500	0.0000	0.0810 (4)	
I8	0.37575 (5)	0.5000	0.20851 (8)	0.0604 (3)	
N9	0.4220 (6)	1.013 (2)	0.9076 (12)	0.094 (4)*	0.5
H9A	0.4115	0.9666	0.9400	0.113*	0.5

H9B	0.4085	1.0744	0.8998	0.113*	0.5
N7	0.4747 (8)	1.0602 (13)	0.8174 (15)	0.094 (4)*	0.5
H7A	0.4982	1.0445	0.7916	0.113*	0.5
H7B	0.4612	1.1217	0.8095	0.113*	0.5
N8	0.4802 (8)	0.8941 (14)	0.8815 (14)	0.094 (4)*	0.5
H8A	0.5037	0.8784	0.8557	0.113*	0.5
H8B	0.4703	0.8482	0.9151	0.113*	0.5
C4	0.4593 (4)	0.9892 (13)	0.8694 (9)	0.094 (4)*	0.5
N14	0.195 (2)	0.591 (4)	0.145 (3)	0.094 (8)*	0.27 (2)
H14A	0.1950	0.6349	0.1902	0.113*	0.27 (2)
H14B	0.1824	0.6077	0.0841	0.113*	0.27 (2)
C6	0.216 (2)	0.500 (3)	0.170 (3)	0.107 (11)*	0.27 (2)
H6	0.2161	0.4527	0.1216	0.128*	0.27 (2)
N13	0.2352 (14)	0.474 (4)	0.261 (3)	0.094 (8)*	0.27 (2)
H13A	0.2349	0.5179	0.3066	0.113*	0.27 (2)
H13B	0.2487	0.4132	0.2776	0.113*	0.27 (2)
N5	0.4878 (5)	0.5000	0.6087 (9)	0.062 (4)	
H5A	0.5016	0.4422	0.6356	0.075*	0.5
H5B	0.5043	0.5578	0.6279	0.075*	0.5
N6	0.4161 (4)	0.4134 (8)	0.5081 (8)	0.081 (3)	
H6A	0.4293	0.3549	0.5342	0.097*	
H6B	0.3858	0.4149	0.4618	0.097*	
C3	0.4419 (6)	0.5000	0.5386 (11)	0.048 (3)	
N3	0.4250 (7)	0.989 (3)	0.4367 (12)	0.094 (7)*	0.5
H3A	0.4235	0.9216	0.4328	0.113*	0.5
H3B	0.4373	1.0237	0.3986	0.113*	0.5
N4	0.3901 (6)	0.984 (3)	0.5564 (11)	0.092 (7)*	0.5
H4A	0.3886	0.9174	0.5529	0.110*	0.5
H4B	0.3793	1.0167	0.5982	0.110*	0.5
C2	0.4087 (9)	1.0360 (18)	0.4993 (16)	0.072 (7)*	0.5
H2	0.4103	1.1085	0.5033	0.087*	0.5
N1	0.7385 (12)	0.469 (3)	0.220 (2)	0.176 (15)*	0.5
H1A	0.7415	0.4067	0.2011	0.211*	0.5
H1B	0.7557	0.4875	0.2801	0.211*	0.5
N2	0.6823 (9)	0.508 (4)	0.0711 (17)	0.173 (11)*	0.5

H2A	0.6851	0.4458	0.0512	0.208*	0.5
H2B	0.6620	0.5525	0.0310	0.208*	0.5
C1	0.7082 (10)	0.535 (2)	0.1602 (18)	0.081 (8)*	0.5
H1	0.7050	0.6021	0.1814	0.098*	0.5
N12	0.5242 (7)	0.4326 (12)	0.1525 (14)	0.084 (3)*	0.5
H12A	0.4923	0.4454	0.1152	0.101*	0.5
H12B	0.5364	0.3701	0.1572	0.101*	0.5
N10	0.6045 (5)	0.490 (2)	0.2595 (10)	0.084 (3)*	0.5
H10A	0.6244	0.5401	0.2912	0.101*	0.5
H10B	0.6167	0.4276	0.2641	0.101*	0.5
N11	0.5359 (8)	0.6064 (13)	0.1962 (14)	0.084 (3)*	0.5
H11A	0.5040	0.6193	0.1589	0.101*	0.5
H11B	0.5556	0.6561	0.2290	0.101*	0.5
C5	0.5547 (4)	0.5097 (13)	0.2033 (8)	0.084 (3)*	0.5
N15	0.224 (2)	0.569 (4)	0.204 (5)	0.094 (8)*	0.23 (2)
H15A	0.2240	0.5440	0.2590	0.113*	0.23 (2)
H15B	0.2260	0.6359	0.1971	0.113*	0.23 (2)
N16	0.219 (3)	0.409 (4)	0.141 (4)	0.094 (8)*	0.23 (2)
H16A	0.2186	0.3836	0.1964	0.113*	0.23 (2)
H16B	0.2171	0.3689	0.0929	0.113*	0.23 (2)
C7	0.222 (2)	0.508 (4)	0.132 (4)	0.107 (11)*	0.23 (2)
H7	0.2218	0.5362	0.0723	0.128*	0.23 (2)

Table S3. Atomic displacement parameters (Å^2).

	U^{11}	U^{22}	U^{33}	U^{12}	U^{13}	U^{23}
Pb1	0.0392 (3)	0.0382 (3)	0.0419 (3)	−0.0003 (2)	0.0183 (2)	0.0007 (2)
Pb2	0.0367 (2)	0.0404 (2)	0.0406 (2)	−0.00008 (15)	0.01428 (16)	0.00074 (15)
I1	0.0523 (4)	0.0724 (5)	0.0594 (5)	0.0004 (4)	0.0008 (4)	0.0041 (4)
I2	0.0647 (7)	0.0298 (5)	0.1045 (9)	0.000	0.0228 (6)	0.000
I3	0.0643 (5)	0.0802 (5)	0.0607 (5)	−0.0091 (4)	0.0412 (4)	−0.0086 (4)
I4	0.0891 (9)	0.0299 (5)	0.0812 (8)	0.000	0.0138 (7)	0.000
I5	0.0431 (4)	0.0581 (4)	0.0591 (4)	−0.0016 (3)	0.0028 (3)	0.0007 (3)
I6	0.0687 (5)	0.0858 (6)	0.0544 (4)	−0.0052 (4)	0.0366 (4)	−0.0036 (4)
I7	0.0403 (6)	0.0951 (9)	0.0885 (9)	0.0006 (6)	−0.0026 (6)	0.0145 (7)
I8	0.0729 (7)	0.0315 (5)	0.0668 (7)	0.000	0.0108 (5)	0.000

N5	0.054 (8)	0.061 (8)	0.057 (8)	0.000	0.000 (7)	0.000
N6	0.071 (7)	0.057 (6)	0.104 (9)	−0.012 (5)	0.015 (6)	−0.006 (6)
C3	0.044 (8)	0.050 (8)	0.046 (8)	0.000	0.010 (7)	0.000

Table S4. Geometric parameters (Å, °).

Pb1—I1^i	3.1876 (8)	N7—C4	1.3331
Pb1—I1	3.1876 (8)	N8—C4	1.3303
Pb1—I2^i	3.2448 (3)	N14—C6	1.2822
Pb1—I2	3.2448 (3)	C6—N13	1.2823
Pb1—I3^i	3.2129 (7)	N5—C3	1.302 (18)
Pb1—I3	3.2129 (7)	N6—C3	1.304 (12)
Pb2—I3	3.3610 (8)	C3—N6^v	1.304 (12)
Pb2—I4	3.2344 (5)	N3—C2	1.2830
Pb2—I5	3.1146 (8)	N4—C2	1.2822
Pb2—I6	3.0802 (8)	N1—C1	1.2810
Pb2—I7	3.3390 (4)	N2—C1	1.2818
Pb2—I8	3.2474 (5)	N12—C5	1.3332
I2—Pb1^{ii}	3.2448 (3)	N10—C5	1.3333
I4—Pb2^{iii}	3.2344 (5)	N11—C5	1.3305
I7—Pb2^{iv}	3.3390 (4)	N15—C7	1.2830
I8—Pb2^v	3.2474 (5)	N16—C7	1.2820
N9—C4	1.3341		
I1^i—Pb1—I1	180.00 (2)	I6—Pb2—I5	93.91 (3)
I1—Pb1—I2	88.77 (3)	I6—Pb2—I7	87.812 (19)
I1^i—Pb1—I2	91.23 (3)	I6—Pb2—I8	89.08 (3)
I1—Pb1—I2^i	91.23 (3)	I7—Pb2—I3	90.450 (18)
I1^i—Pb1—I2^i	88.77 (3)	I8—Pb2—I3	87.05 (3)
I1^i—Pb1—I3^i	89.76 (2)	I8—Pb2—I7	95.66 (2)
I1^i—Pb1—I3	90.24 (2)	Pb1—I2—Pb1^{ii}	161.98 (4)
I1—Pb1—I3	89.76 (2)	Pb1—I3—Pb2	170.48 (3)
I1—Pb1—I3^i	90.24 (2)	Pb2—I4—Pb2^{iii}	162.61 (5)
I2—Pb1—I2^i	180.0	Pb2—I7—Pb2^{iv}	180.0
I3—Pb1—I2^i	89.20 (3)	Pb2^v—I8—Pb2	163.12 (4)
I3—Pb1—I2	90.80 (3)	N7—C4—N9	120.0
I3^i—Pb1—I2	89.21 (3)	N8—C4—N9	120.0

I3^i—Pb1—I2^i	90.80 (3)	N8—C4—N7	119.9
I3^i—Pb1—I3	180.0	N14—C6—N13	120.5
I4—Pb2—I3	94.71 (3)	N5—C3—N6	121.2 (7)
I4—Pb2—I7	86.54 (2)	N5—C3—N6^v	121.2 (8)
I4—Pb2—I8	177.17 (3)	N6—C3—N6^v	116.6 (15)
I5—Pb2—I3	88.32 (2)	N4—C2—N3	120.5
I5—Pb2—I4	86.36 (3)	N1—C1—N2	120.5
I5—Pb2—I7	172.669 (19)	N12—C5—N10	119.9
I5—Pb2—I8	91.49 (3)	N11—C5—N12	120.1
I6—Pb2—I3	175.59 (3)	N11—C5—N10	120.0
I6—Pb2—I4	89.23 (3)	N16—C7—N15	120.3

Symmetry codes: (i) −x+1/2, −y+1/2, −z+1; (ii) −x+1/2, y−1/2, −z+1; (iii) x, −y, z; (iv) −x+1/2, −y+1/2, −z; (v) x, −y+1, z.
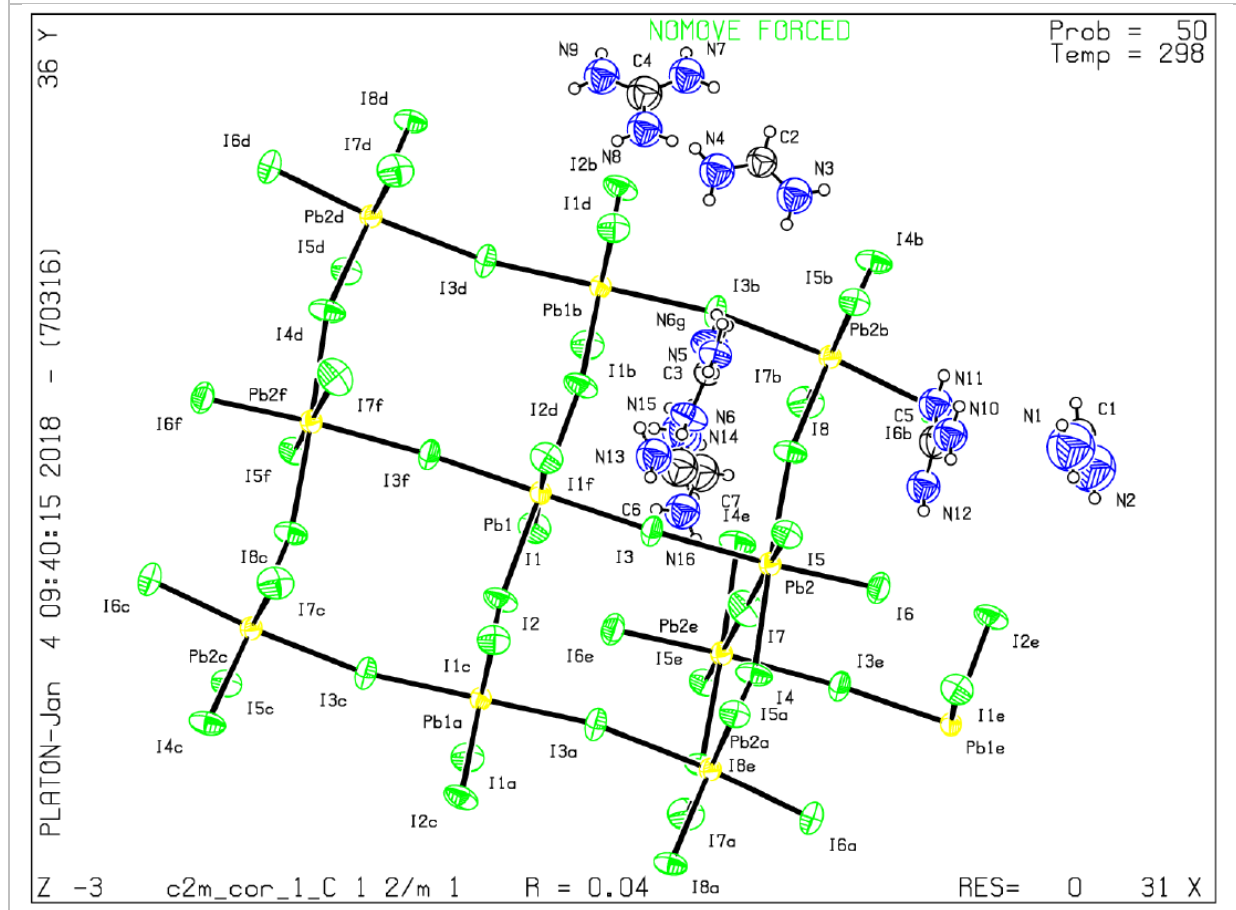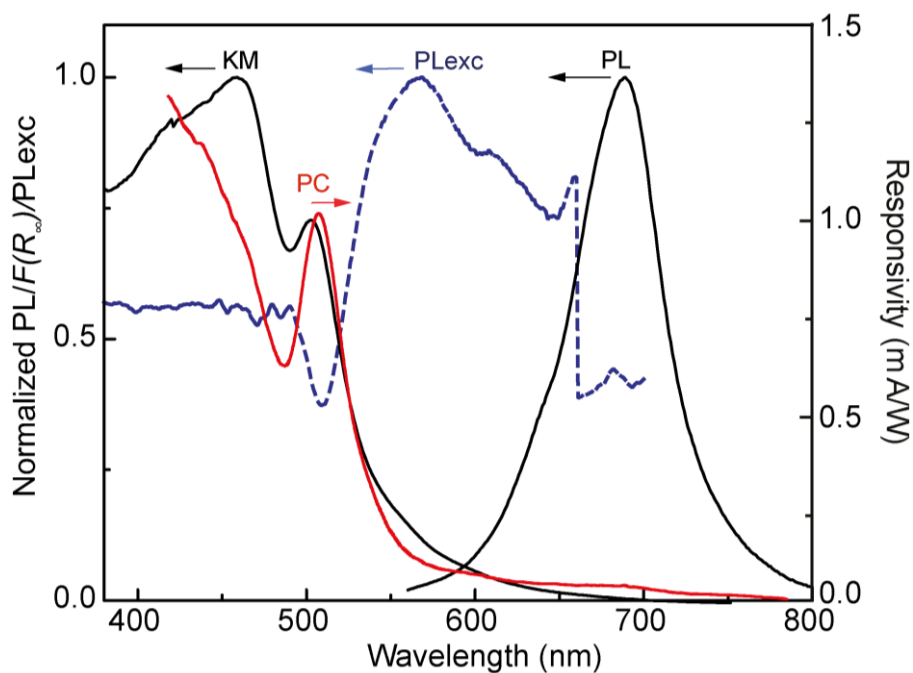
Figure S3. Kubelka–Munk (KM) function $F(R_\infty)=(1-R_\infty)^2/2R_\infty$ (R_∞ - diffusive reflectance), photoluminescence (PL), PL excitation (PLexc) and photoconductivity (PC) spectra of FAGPbI$_4$ (same as shown in Figure 4 of the Main Text). The measurements were performed on the powdered crystals synthesized with a method 1.
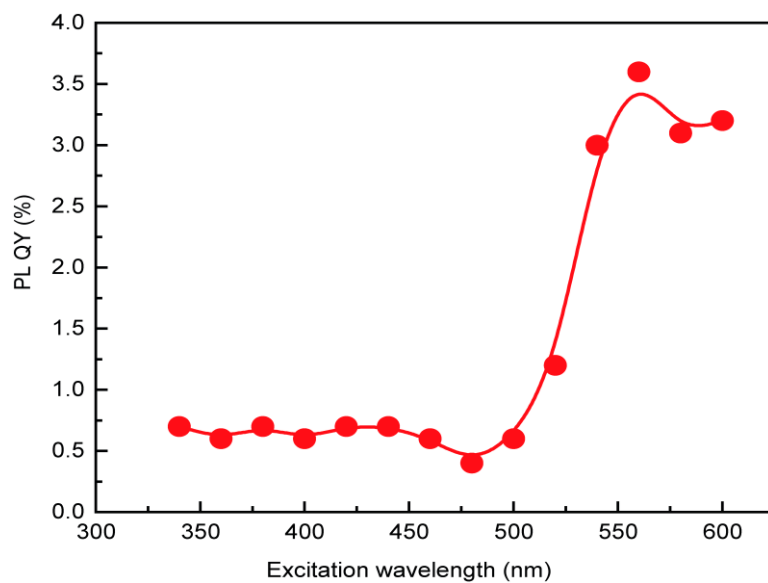
Figure S4. Spectral dependence of PL QY for FAGPbI$_4$. The measurements were performed on the powdered crystals synthesized with a method 1.
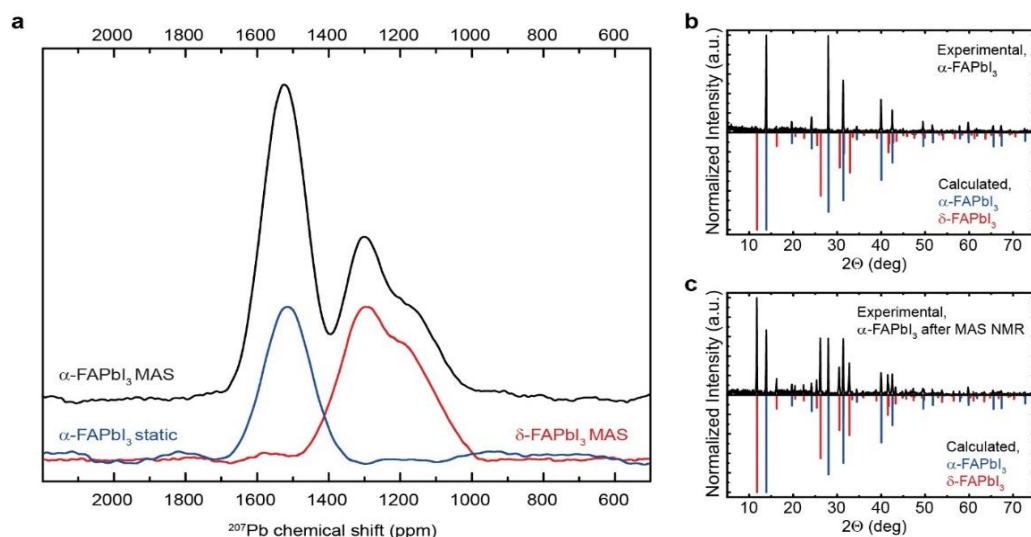
Figure S5. (a) [207]Pb MAS NMR spectrum of α-FAPbI$_3$ (black) showing two different signals. The spectra of α-FAPbI$_3$ in static mode (blue) and of δ-FAPbI$_3$ with MAS are plotted for comparison (red); (b, c) Powder XRD pattern of α-FAPbI$_3$ before and after the MAS NMR measurements, compared to the calculated patterns of α-FAPbI$_3$ (blue) and δ-FAPbI$_3$ (red). The calculated pattern for α-FAPbI$_3$ is based on the experimental single-crystal data reported by M. T. Weller *et. al.* [*J. Phys. Chem. Lett.*, **2015**, 6, 3209-3212]. Both ssNMR and pXRD methods show the formation of δ-FAPbI$_3$ when spinning the sample during NMR experiment. Hence only the static NMR data are truly relevant for comparison with other compounds.

Table S5. [207]Pb ssNMR chemical shifts (referenced to PbMe$_4$) and FWHM of the measured compounds under MAS or, in the case of α-FAPbI$_3$, static mode.

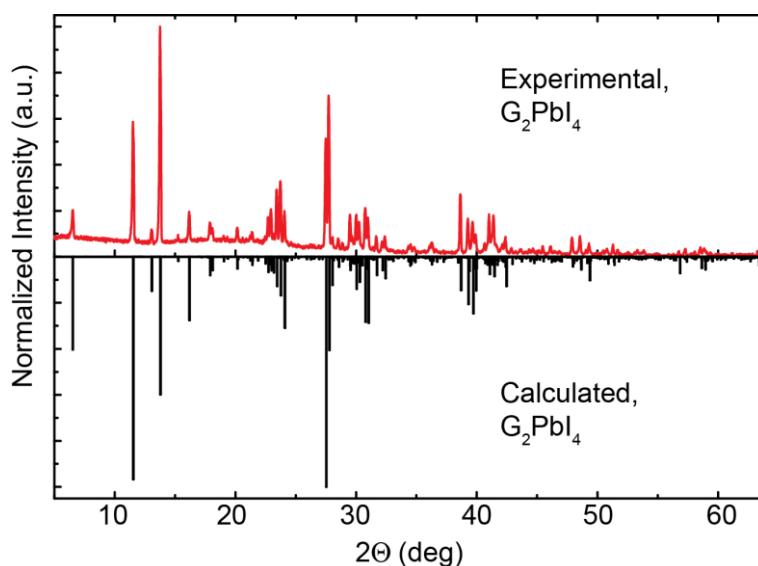| Compound	Chemical shift (ppm)	FWHM (kHz)	Scans	MAS (kHz)
FAGPbI$_4$	1160, 1465	22.4, 20.2	786'432	20
α-FAPbI$_3$	1515	22.2	51'454	0
δ-FAPbI$_3$	1175	21.8	117'702	20
G$_2$PbI$_4$	1515	24.5	131'072	20

Figure S6. The powder XRD pattern of G$_2$PbI$_4$. The calculated pattern is based on the experimental single-crystal XRD data reported by M. Szafranski and A. Katrusiak [*Phys. Rev.* **2000**, B62 (2), 8787 and ICSD card 92045]. A preferred orientation of the microcrystalline powder is observed through the difference in intensity of certain reflections in the experimental pattern compared to the calculated data due to the fact that G$_2$PbI$_4$ crystallizes in the shape of thin plates, giving rise to preferred orientation on a flat sample holder.
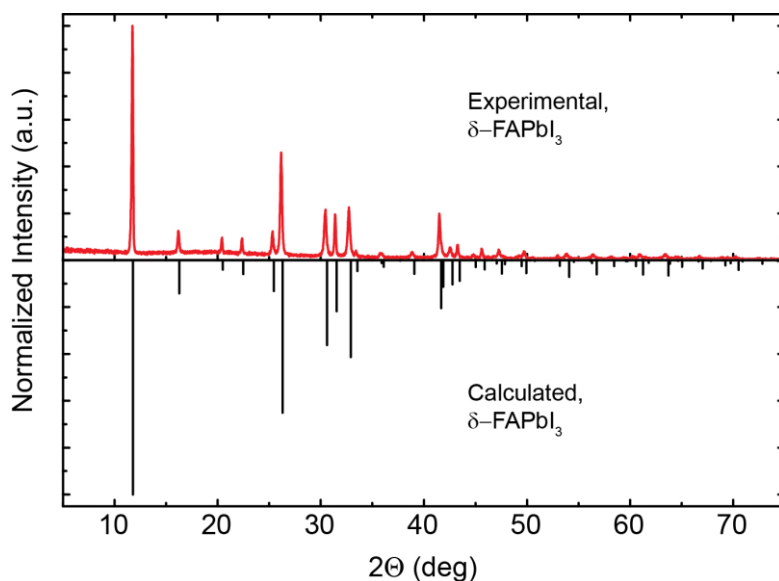
Figure S7. The powder XRD pattern of δ-FAPbI₃ ([CH(NH₂)₂]₂PbI₄, *P*63*mc*). The calculated pattern is based on the experimental single-crystal XRD data reported by C. Stoumpous *et. al.* [*Inorg. Chem.* **2013**, 52, 9019-9038 and ICSD card 250741].
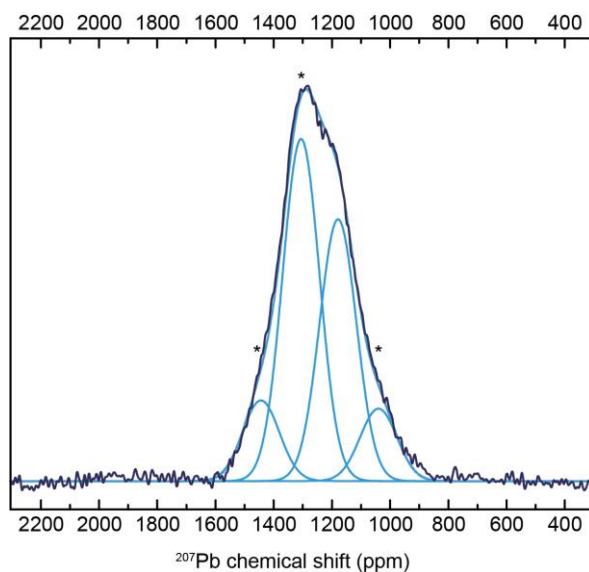

Figure S8. ^{207}Pb MAS NMR spectrum of δ-FAPbI₃ showing a peak at 1175 ppm with a FWHM of 21.8 kHz. The isotropic signal and spinning sidebands were identified by varying the MAS frequency. The peak remaining at the same chemical shift was identified to be the isotropic signal whereas the spinning sidebands (marked by asterisk) are shifting according to the spinning speed. The spectrum was acquired with 117 702 scans. Fitted spinning sidebands and their sum are shown in blue. For the fit the separation between the individual Gaussian peaks was set to 20 kHz.
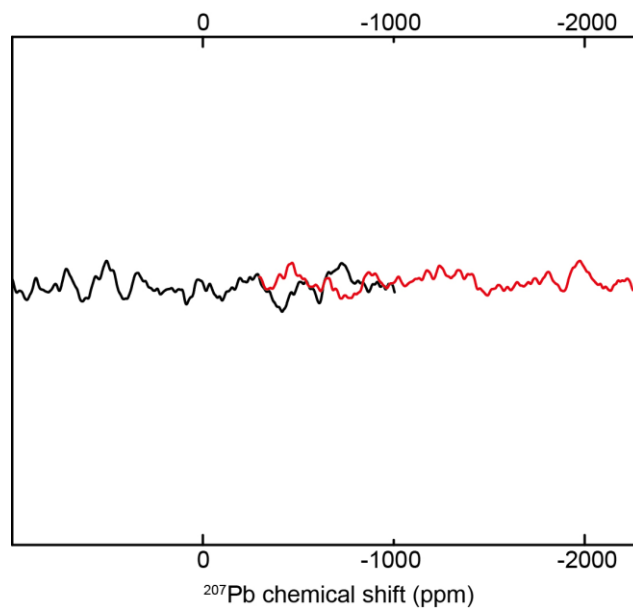
Figure S9. [207]Pb MAS NMR spectra of FAGPbI$_4$ spectral regions around 0 and -1300 ppm. The number of scans acquired were 5000 and 12 536, respectively. The recycle delay was set to 2 seconds to detect impurities with longer relaxation times. No signal could be detected in this spectral range.
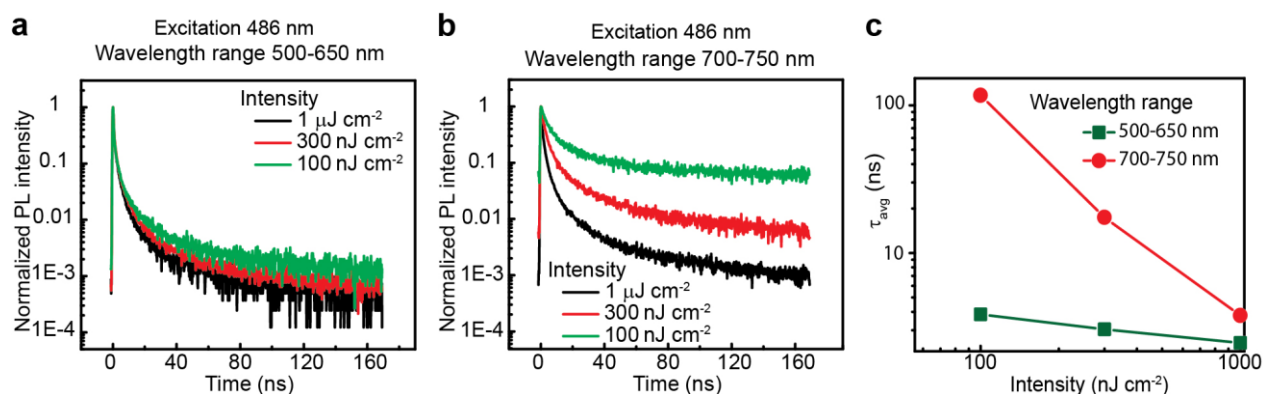

Figure 10. (a, b) Time-resolved PL traces for 500-650 nm and 700-750 nm spectral regions recorded at different excitation intensities on powdered crystals synthesized with method 1. (c) Corresponding average lifetime calculated from TRPL traces for 500-650 nm and 700-750 nm spectral regions from (a, b).
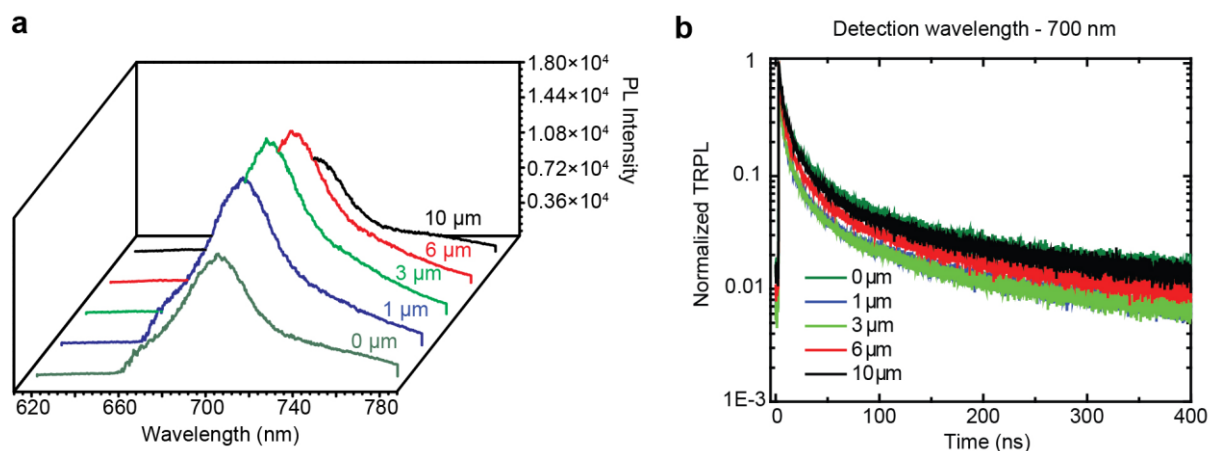

Figure S11. Analysis of PL and TRPL of a single crystal with micrometer spatial resolution.

In order to clarify the complexity of the emission spectrum, and, in particular, to check whether different emission bands originate from spatially-separated emitting centers, we performed PL and TRPL on a home–built micro-photoluminescence setup. In these experiments, a FAGPbI$_4$ single crystal was placed on thin (150 μm) glass coverslip

and excited by a laser diode at 405 nm (repetition rate = 2.5 MHz; excitation power density = 90 $\mu J/cm^2$). In most studied crystal areas, the PL spectrum is composed by different bands and the PL line shape does not strongly depend on the particular spatial location (Figure S11a). TRPL experiments (detection wavelength sets at 700 nm) reveal a modest change of the average lifetime for the different spatial locations (Figure S11b). Given our experimental spatial resolution of a few μm, it is difficult to draw final conclusions concerning the origin of the different emission bands: whether they are associated with some local crystal distortions, free and/or self-trapped excitons, or colour centers.
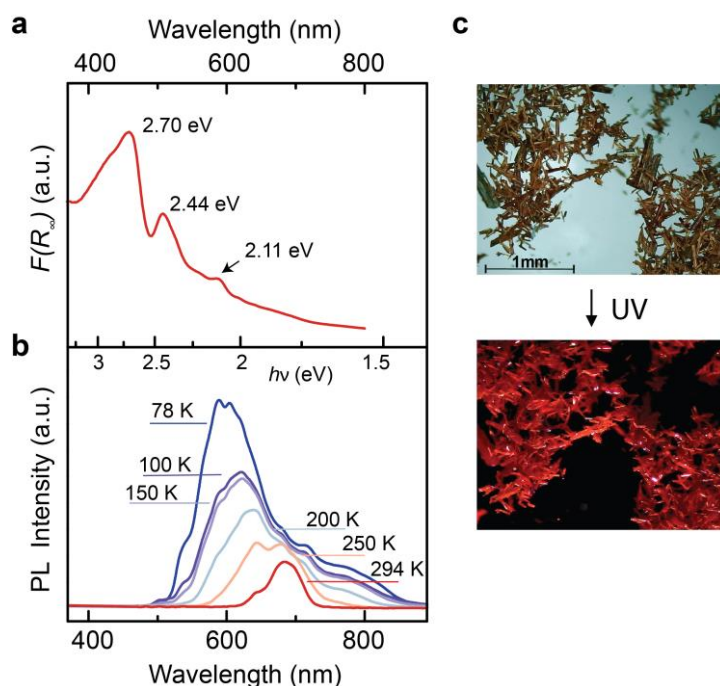

Figure S12. (a) Kubelka–Munk function $F(R_\infty)=(1-R_\infty)^2/2R_\infty$ (R_∞ - diffusive reflectance) of FAGPbI$_4$ on powdered crystals prepared with method 2 and a temperature dependent PL spectra of the same sample (b). (c) A photo of crystals prepared with a higher-yield method 2 under day light (top) and UV illumination (bottom). The absorption and PL spectra showed different intensities of certain transitions, compared to the spectra obtained on powdered crystals synthesized with method 1. For instance, the Kubelka–Munk function shows a large tail that goes roughly from 2.44 down to around 1.7 eV. The transition at 2.11 eV is clearly observable, while for larger crystals (Figure 2e) it was less pronounced. It is hard to make a definite conclusion as to the origin of the transition at 2.11 eV. Supposedly it originates from defects from the surface (microcrystalline powders possess higher surface areas).

Supporting References:

1.   Saidaminov, M. I.; Abdelhady, A. L.; Maculan, G.; Bakr, O. M., Retrograde solubility of formamidinium and methylammonium lead halide perovskites enabling rapid single crystal growth. *Chem. Commun.* **2015,** *51* (100), 17658-17661.
2.   BrukerAXS *APEX3*, v2017.3-0; 2017.
3.   Sheldrick, G. M., A short history of SHELX. *Acta Cryst. A* **2008,** *64*, 112-122.
4.   Sheldrick, G. M., Crystal structure refinement with SHELXL. *Acta Crystallogr. C* **2015,** *71*, 3-8.
5.   Dolomanov, O. V.; Bourhis, L. J.; Gildea, R. J.; Howard, J. A. K.; Puschmann, H., OLEX2: a complete structure solution, refinement and analysis program. *J. Appl. Crystallogr.* **2009,** *42*, 339-341.